

# Anomalous Energy Injection in Turbulent Neutron Star Cores

Anirudh Sivakumar,<sup>1</sup> Pankaj Kumar Mishra,<sup>2</sup> Ahmad A. Hujeirat,<sup>3</sup> and Paulsamy Muruganandam<sup>1,4</sup>

<sup>1</sup>Department of Physics, Bharathidasan University, Tiruchirappalli 620 024, Tamil Nadu, India

<sup>2</sup>Department of Physics, Indian Institute of Technology Guwahati, Guwahati 781039, Assam, India

<sup>3</sup>Interdisciplinary Center for Scientific Computing, The University of Heidelberg, 69120 Heidelberg, Germany

<sup>4</sup>Department of Medical Physics, Bharathidasan University, Tiruchirappalli 620 024, Tamil Nadu, India

(Dated: June 26, 2025)

Neutron star glitches—sudden increases in rotational frequency—are thought to result from angular momentum transfer via quantized vortices in the superfluid core. Using a two-dimensional rotating atomic Bose-Einstein condensate with phenomenological damping and a pinning potential to mimic the crust, we model the dynamics underlying these events. Our simulations reveal a transient Kolmogorov-like turbulent cascade ( $k^{-5/3}$ ) that transitions to a Vinen-like scaling ( $k^{-1}$ ). We identify an anomalous secondary injection mechanism driven primarily by quantum pressure, which sustains turbulent fluctuations in pulsar glitches. By tuning the damping coefficient  $\gamma$ , we determine an optimal regime for energy transfer. These findings provide a robust analogy for neutron star glitch phenomena and offer new insights into turbulence in extreme astrophysical environments.

**Introduction:** Decaying neutron stars exhibit sudden increases in rotation frequency, known as glitches [1], caused by the transfer of angular momentum from quantized vortices in the neutron superfluid to the outer crust of the pulsar [2, 3]. This transfer is primarily triggered by the vortex avalanche mechanism, in which quantum vortices become pinned to crustal nuclei [4], preventing the superfluid from spinning down at the same rate as the crust. The resulting rotational lag between the crust and superfluid generates a Magnus force on the vortices [5]. Once a critical velocity is reached, the quantized vortices unpin from their pinning sites [6]. These vortices are then expelled toward the crust, transferring their angular momentum and producing a glitch [7]. This glitch process involves a complex vortex avalanche encompassing millions of vortices, triggering their depinning [8].

Modeling the depinning avalanche mechanism poses significant challenges. Vortex depinning initiates when a vortex, initially trapped by a pinning site, overcomes the attractive force and begins moving in the direction of the applied superfluid flow. Several factors, such as the critical velocity of the superfluid flow and the size and shape of the pinning site, affect the overall dynamics of depinning [9]. However, an alternative analysis suggests that glitches emerge due to a quantum transition in which the core transforms into a superconducting gluon-quark superfluid state, with resultant vortex depinning occurring at the boundary layer between the core and the surrounding dissipative medium [3]. In this letter, we demonstrate the presence of anomalous energy transfer from quantum pressure to incompressible kinetic energy in the turbulent state of the neutron star core, which sustains pulsar glitches.

In recent years, rotating Bose-Einstein condensates (BECs) have been widely employed to model the dynamics of quantized vortices in different astrophysical systems, such as neutron superfluids in strong gravitational wells [10–12], turbulent dark matter [13], pulsar glitches [14]. Verma *et al.* [15] and Shukla *et al.* [14] developed a minimal model for the emergence of the superfluid glitches based on the interaction of the neutron-superfluid vortices and proton-superconductor flux tubes. The inherent compressibility of the BECs renders

them susceptible to quantum turbulence (QT) under dynamic instabilities. This turbulence is primarily characterized by the breakdown of vortices in a self-similar process, manifesting as a power-law scaling of  $k^{-5/3}$  [16, 17], known as the Kolmogorov spectrum. In addition to the Kolmogorov regime, QT in BECs also exhibits Vinen turbulence, characterized by random vortex distributions in superfluids, indicated by a  $k^{-1}$  scaling. Novel turbulence regimes have been identified in recent years, including strong quantum turbulence [18, 19], marked by density fluctuations and non-polarized vortex lines; rotational quantum turbulence [20–23]; and turbulence in self-gravitating dark-matter BEC candidates [13, 24].

Previous studies have explored the nature of glitches and vortex avalanches in the context of pinning potentials and superfluid behavior. However, the role of superfluid-crust interactions in inducing turbulent flow remains largely unexamined. In this letter, we investigate the characteristics of turbulence and associated velocity flows arising from such interactions. Furthermore, it analyzes the mechanisms driving this turbulence, facilitated by pinning sites and the dynamic spin-down of the condensate. The damping effects on the system are also evaluated, identifying an optimal damping coefficient that maximizes turbulence strength. Recent studies indicate that quantum turbulence suppresses collective excitation modes in BECs [25, 26]. As these modes drive vortex avalanches and glitch phenomena, quantifying the onset of turbulence in such systems is essential.

**The Model:** We model the interior of a spinning-down neutron star's superfluid core using a quasi-two-dimensional (quasi-2D) atomic Bose-Einstein condensate. This rotating BEC system, incorporating dissipative interactions, is described by the damped Gross-Pitaevskii equation (dGPE), presented in its non-dimensional form in Ref. [27].

$$(i - \gamma) \frac{\partial \psi}{\partial t} = \left[ -\frac{1}{2} \nabla^2 + V(\mathbf{r}, t) + g|\psi|^2 - \Omega(t)L_z \right] \psi, \quad (1)$$

where  $\psi \equiv \psi(\mathbf{r}, t)$  is the condensate wave function, with  $\mathbf{r} \equiv (x, y)$ .  $\nabla^2 = \partial_x^2 + \partial_y^2$  represents the two-dimensional Laplacian,  $\gamma$  corresponds to the parameterized damping coefficient,

and  $g$  is the nonlinear interaction strength given by  $g = 800$ . The time-dependent rotation frequency  $\Omega(t)$  describes the rotational deceleration profile of the condensate as follows:

$$\Omega(t) = \begin{cases} \Omega_0 \cos^2\left(\frac{\pi t}{2t_s}\right), & \text{if } t \leq t_s, \\ 0, & \text{if } t > t_s, \end{cases} \quad (2)$$

where  $\Omega_0$  is the initial rotation frequency of the condensate, and  $t_s$  is the spin-down time. The  $z$ -component of the angular momentum is given by  $L_z = i\hbar(y\partial_x - x\partial_y)$ .

The potential term  $V(\mathbf{r}, t)$  comprises the following components

$$V(\mathbf{r}, t) = V_{\text{box}}(\mathbf{r}) + V_{\text{crust}}(\mathbf{r}, t) + V_{\text{cent}}(\mathbf{r}, t). \quad (3)$$

The confining circular-box potential,  $V_{\text{box}}$ , with radius  $R_{\text{box}}$ , is defined as  $V_{\text{box}}(\mathbf{r}) = V_{0b}\Theta(r - R_{\text{box}})$  [27], where  $\Theta$  is the Heaviside step function and  $r = \sqrt{x^2 + y^2}$ . For our analysis, we set the barrier height and radius of the circular-box trap as  $V_{0b} = 100$  and  $R_{\text{box}} = 6$ , respectively. The crust potential, which acts as a vortex pinning site, is given by [14, 15]:

$$V_{\text{crust}}(\mathbf{r}, t) = V_{0c} \exp\left(-\frac{(|\mathbf{r}_p| - r_{\text{crust}})^2}{(\Delta r_{\text{crust}})^2}\right) \tilde{V}(x_\theta, y_\theta), \quad (4)$$

where  $\tilde{V}(x_\theta, y_\theta) = 3 + \cos(n_{\text{crust}}x_\theta) + \cos(n_{\text{crust}}y_\theta)$ , and the rotated coordinates are  $x_\theta = \cos(\theta(t))x_p + \sin(\theta(t))y_p$  and  $y_\theta = -\sin(\theta(t))x_p + \cos(\theta(t))y_p$ . Here,  $n_{\text{crust}}$  determines the number of pinning sites,  $r_{\text{crust}}$  is the radius at which  $V_{\text{crust}}$  is maximized, and  $\Delta r_{\text{crust}}$  represents the crust thickness. The crust potential parameters are based on Refs. [14, 15]. The centrifugal potential,  $V_{\text{cent}}(\mathbf{r}, t) = \frac{1}{2}\Omega(t)^2 r^2$ , ensures uniform condensate density under rotation. Following Refs. [27–29], we adopt a coherent length scale of  $\xi = 10$  fm, yielding an energy scale of  $\varepsilon = 207$  keV. With these parameters, the time scale is calculated as  $\tau = 3.2 \times 10^{-21}$  s. We compute the kinetic energy components and their spectra based on the analysis of their numerical implementation in Ref. [30]. The simulation involves numerically solving the Gross-Pitaevskii equation using the split-step Crank-Nicolson method [31, 32] in a computational domain of size  $512 \times 512$ , with spatial steps  $dx = dy = 0.05$  and a time step  $dt = 10^{-3}$  to ensure numerical stability and convergence. The numerical simulations are performed on an NVIDIA A100 GPU using CUDA C codes developed based on [33]. Initially, we prepare the condensate and crust with an initial rotation frequency  $\Omega_0 = 2$  through imaginary-time iterations ( $t \rightarrow -it$ ). This converged profile is then spun down at varying rates, characterized by the spin-down time  $t_s$ , in real-time. We first consider a case with a static crust and no dissipation ( $\gamma = 0$ ) while exploring the effects of damping in subsequent analyses.

**Results:** Superfluidity significantly impacts the interior dynamics of neutron stars, forming quantized vortices under rotation. These vortices facilitate angular momentum transfer, driving glitch behavior, while the superfluid density provides a qualitative picture of quantized vortices during the spin-down process. The density profiles shown in Fig. 1 indicate that the

centrifugal potential initially dominates over the circular box trap due to the high rotation frequency. As the condensate

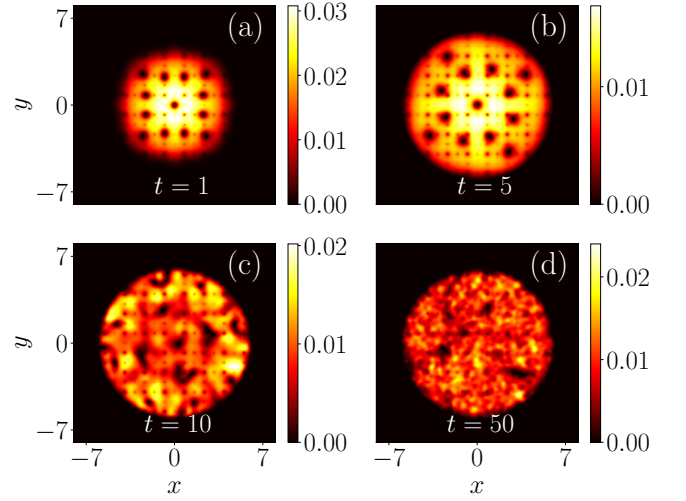


FIG. 1. Snapshots of condensate density during real-time spin-down at  $t_s = 10$  with the crust potential. As the condensate spins down, the initially dominant centrifugal confinement [(a)] is overtaken by the circular box trap [(b)–(d)]. Concurrently, turbulent flow induces the depinning of vortices.

spins down, the influence of the box trap becomes dominant, resulting in a more uniform density distribution. The presence of the crust significantly increases the vortex number by providing pinning sites within the condensate and also accelerates vortex decay through a depinning mechanism. Liu and colleagues [9, 27] attribute this behavior to the Magnus flow generated around the pinning sites of the crust.

The Magnus flow, induced by the spin-down of the condensate, reaches a critical velocity that triggers vortex depinning and simultaneous density fluctuations. As the condensate approaches the spin-down time  $t_s$ , the flow enters a turbulent regime driven by this critical velocity. After spin-down, turbulent fluctuations persist briefly before decaying due to the absence of external forcing.

Further, the vortex avalanche triggered by Magnus flow results in an instantaneous recoupling of the superfluid and normal components, accompanied by a rapid transfer of angular momentum. This abrupt transition in superfluid systems may induce turbulence but cannot be confirmed using density profiles alone. To characterize the turbulent flow in the system, we therefore analyze the incompressible and compressible kinetic energy spectra of the condensate. We characterize the turbulent regimes by using Thomas-Fermi radius  $R_{TF}$ , the inter-vortex distance  $\ell_0$ , and the healing length  $\xi$ . For two-dimensional systems, the inter-vortex distance is approximated as  $\ell_0 = 1/\sqrt{l_v}$ , where  $l_v$  represents the vortex density per unit area.

In the turbulent regime, the incompressible kinetic energy spectrum exhibits a  $k^{-5/3}$  scaling in the inertial range  $2\pi/R_{TF} < k < 2\pi/\ell_0$  [see Figs. 2(a) and 2(c)], associated with vortex breakdown. Additionally, the condensate enstrophy

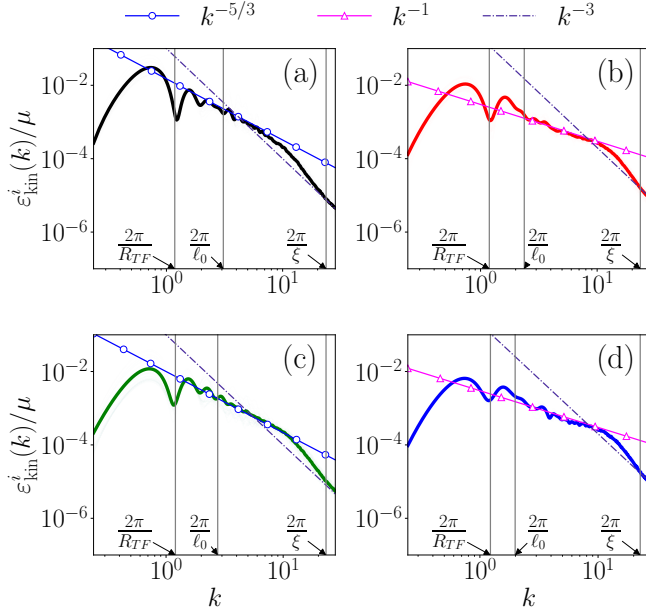


FIG. 2. Incompressible kinetic energy spectra exhibiting the Kolmogorov cascade for spin-down time  $t_s = 10$  (a), averaged over  $t = 10$  to  $t = 30$ ; (b) averaged over  $t = 30$  to  $t = 50$ , and spin-down time  $t_s = 20$  (c) averaged over  $t = 20$  to  $t = 50$ ; and (d) averaged over  $t = 50$  to  $t = 60$ . The spectra initially [(a) and (c)] and later durations [(b) and (d)] exhibit  $k^{-5/3}$  and  $k^{-1}$  scalings, respectively alongside a  $k^{-3}$  scaling.

undergoes a self-similar cascade, manifested as a  $k^{-3}$  power-law scaling at large  $k$  values in the incompressible spectrum. For longer spin-down times, the  $k^{-5/3}$  scaling weakens, while the  $k^{-3}$  scaling becomes more pronounced. The observation that turbulent instability is triggered by rapid transitions in angular frequency and that the energy cascade extends beyond the intervortex spacing aligns with findings on rotational two-dimensional quantum turbulence under varying rotation frequencies [22].

Following the initial turbulent behavior exhibiting a Kolmogorov cascade, the vortex system transitions to a Vinen turbulence phase as several vortices decay due to the spin-down. This Vinen turbulence is characterized by a  $k^{-1}$  power-law scaling in the range  $k > 2\pi/\ell_0$  [see Fig. 2(b) and 2(d)], where individual vortices dominate the velocity field. Notably, the intervortex spacing decreases as vortex density declines, enabling the  $k^{-1}$  scaling to manifest at these length scales. Similar to the Kolmogorov regime, the  $k^{-1}$  scaling is more pronounced for shorter spin-downs (smaller  $t_s$  values).

As the condensate spins down, the vortex population decreases, reducing the vortex-line density  $l_v$ . For 2D systems,  $l_v$  can be approximated by computing the vortex population over a given area, which leads to increased intervortex spacing  $\ell_0$  from the Kolmogorov to the Vinen regime. As shown in Fig. 3, the vortex density exhibits a distinct scaling behavior with respect to time, further confirming the turbulent behavior of the condensate. During the initial Kolmogorov turbulent

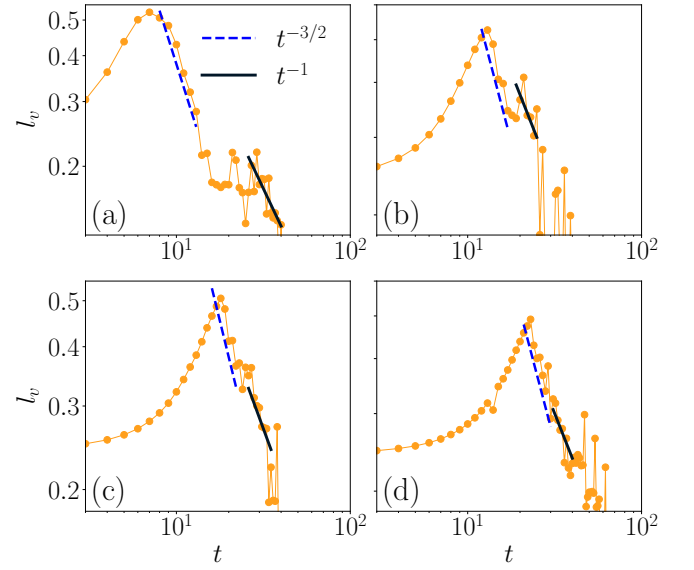


FIG. 3. Variation of vortex density (per unit area) with respect to time on a logarithmic scale for spin-down times (a)  $t_s = 10$ , (b)  $t_s = 20$ , (c)  $t_s = 30$ , and (d)  $t_s = 40$ . The vortex decay in the Kolmogorov and Vinen turbulence regimes exhibits  $t^{-3/2}$  and  $t^{-1}$  scaling behaviors, respectively.

regime, the vortex-line density  $l_v$  scales as  $t^{-3/2}$ , transitioning to  $t^{-1}$  scaling in the later Vinen turbulent regime. This temporal decay of vortex-line density is attributed to vortex breakdown in the Kolmogorov regime, as well as to sound radiation (Kelvin-wave emission) and vortex reconnection in the Vinen regime [34–36]. For shorter spin-down times, the  $t^{-3/2}$  scaling persists over a longer timescale, corresponding to a broader spatial extent of the  $k^{-3/2}$  scaling in the incompressible kinetic energy spectrum (Fig. 2).

Despite the spatial and temporal profiles of energy and vortex density indicating turbulent behavior, the onset of turbulence after the condensate spins down requires further investigation. We analyze the temporal behavior of the kinetic energy components and observe that the incompressible kinetic energy (associated with vortex flow) initially dominates but decreases as the condensate spins down without rotational forcing to inject vortices into the system. The quantum pressure energy, which is not associated with the velocity flow of the condensate, becomes dominant over the incompressible component. The spin-down time marks the crossover point where the quantum pressure component surpasses the incompressible component, beyond which Kolmogorov turbulence is observed in the condensate. This finding contrasts with turbulent decay in self-gravitating condensates, as reported in Ref. [13], where the dominance of the quantum pressure component indicates the absence of turbulence. This discrepancy is attributed to differences in the turbulent decay mechanisms. In the self-gravitating case, the decay of incompressible kinetic energy results from the instantaneous expulsion of vortex structures, whereas in the spin-down case, it arises from

more gradual vortex decay. Despite reaching the spin-down time, vortices persist in the condensate (see Fig. 1) for a sufficient duration to undergo an energy cascade and exhibit turbulent behavior.

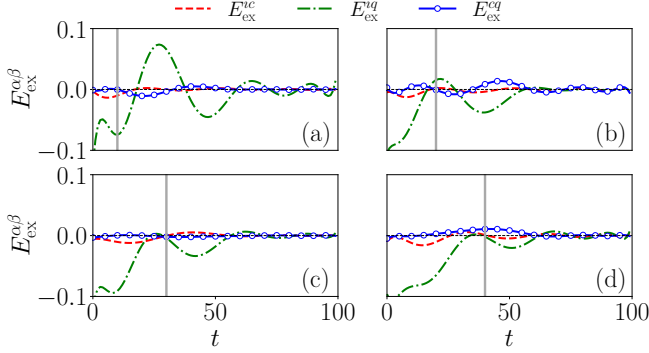


FIG. 4. Temporal profiles of the total kinetic energy exchange between its components for spin-down times (marked by dark-grey vertical lines) (a)  $t_s = 10$ , (b)  $t_s = 20$ , (c)  $t_s = 30$ , and (d)  $t_s = 40$ . The red dashed line represents energy transfer from the incompressible to the compressible component ( $E_{\text{ex}}^{ic}$ ), the green dash-dotted line represents energy transfer between the incompressible and quantum pressure components ( $E_{\text{ex}}^{iq}$ ), and the blue line with circles represents energy transfer between the compressible and quantum pressure components ( $E_{\text{ex}}^{cq}$ ). A negative exchange energy indicates a transfer from the first component  $\alpha \in \{i, c, q\}$  in the superscript to the second  $\beta \in \{i, c, q\}$ , while a positive value indicates the reverse.

Although glitch events are explained by the transfer of angular momentum [37], analyzing the onset of turbulence and the dynamics of quantized vortices is required to fully understand the transport of kinetic energy components, which, in turn, enables a new perspective on vortex depinning. The evolution of net energy transport between the kinetic components, shown in Fig. 4, provides critical insight into the post-spin-down dynamics and explains the persistence of vortex flow. The energy exchange between the compressible–quantum pressure and incompressible–compressible components does not significantly influence the turbulent dynamics. However, the energy exchange between the incompressible and quantum pressure components, denoted  $E_{\text{ex}}^{iq}$ , is initially negative, indicating energy transfer from the incompressible to the quantum pressure component. After the condensate spins down,  $E_{\text{ex}}^{iq} \rightarrow 0$ , as no further incompressible energy is transferred to quantum pressure. For sufficiently short spin-down times [see Fig. 4(a)–(b)], the exchange energy becomes positive, indicating an injection of incompressible energy from the quantum pressure component. This secondary injection mechanism sustains turbulent behavior in the condensate, even after the loss of rotational forcing, which explains the existence of vortex flow after the spin-down time is reached. For longer spin-down times, the peak of the secondary injection diminishes, reducing the intensity of turbulence.

The damping coefficient  $\gamma$  is used in atomic BECs to model

vortex-sound interactions [38]. A comparable approach is employed in neutron star interiors to describe interactions with the outer crust and proton superconducting core. In addition, the impact of  $\gamma$  on vortex and turbulent dynamics under the dGPE model provides an important clue to the contribution of the interaction between neutron star interiors, which are mainly composed of superfluid and proton superconductors. For atomic BECs, the damping parameter  $\gamma$  can be controlled by varying the temperature of the condensate, significantly affecting the vortex and density-wave dynamics. The damping parameter  $\gamma$  is controlled by varying the temperature of the condensate, significantly affecting vortex and density-wave dynamics. Figure 5 illustrates the evolution of incompress-

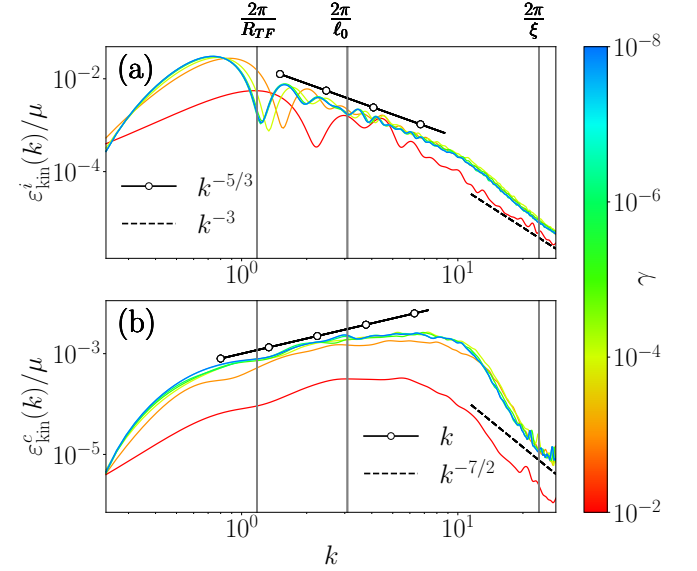


FIG. 5. Variation of (a) incompressible kinetic energy spectra and (b) compressible kinetic energy spectra for different values of the damping coefficient  $\gamma$ . Both spectra are calculated for the case  $t_s = 10$  and averaged over the time range  $t = 10$  to  $t = 30$ . The spectra exhibit a better fit to turbulent scaling for smaller  $\gamma$  values.

ible and compressible kinetic energy spectra for various values of the damping coefficient  $\gamma$ . For the strongly turbulent case with  $t_s = 10$  [see Figs. 2(a)], the spectra exhibit pronounced  $k^{-5/3}$  scaling in the incompressible component and  $k$  scaling in the compressible component for smaller damping values (underdamped regime). The  $k$  scaling in the infrared region and  $k^{-7/2}$  scaling in the ultraviolet regime for the compressible spectra indicates the presence of weak wave turbulence [13, 20, 23]. At approximately  $\gamma \approx 10^{-2}$ , the spectra abruptly lose their scaling behavior as stronger damping (overdamped regime) dissipates the turbulent flow. This turbulent flow is further confirmed by the emergence of a prominent  $k^{-3}$  scaling and the diminishing  $k^{-5/3}$  scaling in the overdamped case ( $\gamma \approx 10^{-2}$ ), indicating the inhibition of vortex breakdown and the formation of a stable vortex lattice structure. It is worthwhile to mention mainly an over-damped condensate ( $\gamma > 0.02$ ) has been considered to model superfluid



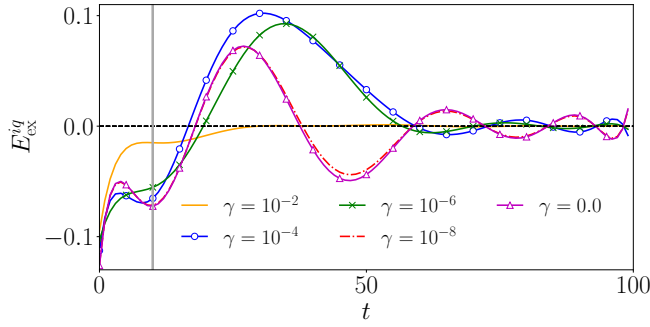


FIG. 6. Time evolution of the exchange energy between the incompressible and quantum pressure components for spin-down time  $t_s = 10$  (dark-gray vertical line). The different curves represent the behavior of the profile under varying damping strengths  $\gamma$ . Notably, the injection of incompressible energy is maximized for an optimal damping coefficient, corresponding to neither underdamped nor overdamped conditions.

cores of neutron stars due to several potential dissipation pathways [8, 12].

Similar to the non-damped case, we complement the spectral analysis with the exchange energy profile in the presence of damping Fig. 6. The injection of incompressible kinetic energy reaches a maximum at an optimal value of  $\gamma$ , situated between the underdamped and overdamped regimes. Under these optimal damping conditions, the transfer of energy from quantum pressure to incompressible modes appears to be significantly enhanced. Given that  $\gamma$  serves as a simplified parametrization of dissipation in quantum fluids, the underlying mechanism responsible for the observed maximum in incompressible energy injection at this intermediate damping requires further investigation. In the overdamped regime, around  $\gamma \approx 10^{-2}$ , the positive peak in exchange energy is absent, consistent with the suppression of turbulence under such strongly dissipative conditions.

**Summary and Conclusion:** We investigated two-dimensional quantum turbulence in a spinning-down condensate subjected to a crust potential that provides vortex pinning sites. By analyzing a continuous spin-down profile, we demonstrated that as the spin-down duration  $t_s$  approaches the quasi-discrete limit, the condensate exhibits turbulent behavior. Following the spin-down duration  $t_s$ , the neutron star core displays turbulence characterized by an incompressible kinetic energy spectrum with a  $k^{-5/3}$  scaling, indicative of the Kolmogorov regime, and a compressible energy spectrum with a  $k^1$  scaling, consistent with thermalization. The turbulent core subsequently transitions to the Vinen regime, marked by a  $k^{-1}$  scaling, where isolated vortices dominate the flow. In both regimes, the scaling behavior weakens as the spin-down duration increases. The vortex-line density  $l_v$  exhibits a power-law decay, scaling as  $t^{-3/2}$  in the Kolmogorov regime and as  $t^{-1}$  in the Vinen regime.

The interplay between kinetic energy components reveals that spinning down induces an energy transfer from the in-

compressible component to quantum pressure. After the spin-down, a reverse transfer from quantum pressure to incompressible energy occurs, which is sufficient to trigger a turbulent cascade after the cessation of rotational forcing. This injection of kinetic energy is indirectly observed in the vortex-line decay profile as an increase in vortex-line density around  $t_s$ , resulting from the transfer of energy back into the incompressible component. This behavior is attributed to the depinning of vortex lattice, leading to a vortex avalanche [8, 39, 40].

The variation of the Kolmogorov spectrum and compressible spectrum with the damping parameter  $\gamma$  shows a sharp transition from non-turbulent to turbulent scaling behavior occurs near  $\gamma \sim 10^{-2}$ . We have also observed an optimal damping coefficient, where the transfer from quantum pressure to incompressible energy is maximized. Under longer spin-down durations, Liu *et al.* [27] have reported pulsar glitches triggered by vortex avalanches. As quantum turbulence has been shown to suppress collective excitations in condensates [25, 26], the parameters determining the onset of turbulence presented here may be relevant to glitch formation in the presence of a crust potential. While vortex depinning is commonly considered the mechanism behind glitches in crust-bound systems, self-gravitating BECs without pinning potentials can also exhibit vortex expulsion to the periphery when the total circulation exceeds a critical threshold  $\xi_c$  [13, 41]. Such expulsions could similarly interact with an external crust and trigger glitch-like behavior in the absence of depinning.

Turbulence significantly influences pulsar glitch phenomena via spin-down profiles and dissipative interactions, providing essential insights into the internal dynamics of neutron stars. This study is particularly valuable for exploring inhomogeneous two-dimensional quantum turbulence and its associated dynamics, especially the emergence of a secondary energy injection mechanism.

The work of P.M. is supported by the Ministry of Education-Rashtriya Uchchatar Shiksha Abhiyan (MoE RUSA 2.0): Bharathidasan University – Physical Sciences.

- 
- [1] V. Radhakrishnan and R. Manchester, Detection of a Change of State in the Pulsar PSR 0833-45, *Nature* **222**, 228 (1969).
  - [2] R. N. Manchester, Pulsar glitches, *IAU Symp.* **337**, 197 (2017).
  - [3] A. A. Hujeirat, Glitches: The exact quantum signatures of pulsars metamorphosis, *J. Mod. Phys.* **09**, 554 (2018).
  - [4] N. Chamel and P. Haensel, Physics of neutron star crusts, *Living Rev. Relativ.* **11**, 10 (2008).
  - [5] E. B. Sonin, Magnus force in superfluids and superconductors, *Phys. Rev. B* **55**, 485 (1997).
  - [6] O. R. Stockdale, M. T. Reeves, and M. J. Davis, Dynamical mechanisms of vortex pinning in superfluid thin films, *Phys. Rev. Lett.* **127**, 255302 (2021).
  - [7] A. Melatos, C. Peralta, and J. S. B. Wyithe, Avalanche dynamics of radio pulsar glitches, *Astrophys. J.* **672**, 1103 (2008).
  - [8] J. R. Lönnborn, A. Melatos, and B. Haskell, Collective, glitch-like vortex motion in a neutron star with an annular pinning barrier, *Mon. Not. R. Astron. Soc.* **487**, 702 (2019).

- [9] I.-K. Liu, S. B. Prasad, A. W. Baggaley, C. F. Barenghi, and T. S. Wood, Vortex depinning in a two-dimensional superfluid, *J. Low Temp. Phys.* **215**, 376 (2024).
- [10] A. B. Migdal, Superfluidity and the moments of inertia of nuclei, *Nucl. Phys.* **13**, 655 (1959).
- [11] L. Warszawski and A. Melatos, Gross-Pitaevskii model of pulsar glitches, *Mon. Not. R. Astron. Soc.* **415**, 1611 (2011).
- [12] L. Warszawski, A. Melatos, and N. G. Berloff, Unpinning triggers for superfluid vortex avalanches, *Phys. Rev. B* **85**, 104503 (2012).
- [13] A. Sivakumar, P. K. Mishra, A. A. Hujeirat, and P. Muruganandam, Revealing turbulent dark matter via merging of self-gravitating condensates, *Phys. Rev. D* **111**, 083511 (2025).
- [14] S. Shukla, M. E. Brachet, and R. Pandit, Neutron-superfluid vortices and proton-superconductor flux tubes: Development of a minimal model for pulsar glitches, *Phys. Rev. D* **110**, 083002 (2024).
- [15] A. K. Verma, R. Pandit, and M. E. Brachet, Rotating self-gravitating Bose-Einstein condensates with a crust: A model for pulsar glitches, *Phys. Rev. Research* **4**, 013026 (2022).
- [16] M. Kobayashi and M. Tsubota, Quantum turbulence in a trapped Bose-Einstein condensate, *Phys. Rev. A* **76**, 045603 (2007).
- [17] M. Kobayashi and M. Tsubota, Quantum Turbulence in a Trapped Bose-Einstein Condensate under Combined Rotations around Three Axes, *J. Low Temp. Phys.* **150**, 587 (2008).
- [18] C. F. Barenghi, H. A. J. Middleton-Spencer, L. Galantucci, and N. G. Parker, Types of quantum turbulence, *AVS Quantum Sci.* **5**, 025601 (2023).
- [19] H. A. J. Middleton-Spencer, A. D. G. Orozco, L. Galantucci, M. Moreno, N. G. Parker, L. A. Machado, V. S. Bagnato, and C. F. Barenghi, Strong quantum turbulence in Bose-Einstein condensates, *Phys. Rev. Research* **5**, 043081 (2023).
- [20] J. A. Estrada, M. E. Brachet, and P. D. Mininni, Turbulence in rotating Bose-Einstein condensates, *Phys. Rev. A* **105**, 063321 (2022).
- [21] J. A. Estrada, M. E. Brachet, and P. D. Mininni, Thermalized Abrikosov lattices from decaying turbulence in rotating BECs, *AVS Quantum Sci.* **4**, 046201 (2022).
- [22] A. Sivakumar, P. K. Mishra, A. A. Hujeirat, and P. Muruganandam, Energy spectra and fluxes of turbulent rotating Bose-Einstein condensates in two dimensions, *Phys. Fluids* **36**, 027149 (2024).
- [23] A. Sivakumar, P. K. Mishra, A. A. Hujeirat, and P. Muruganandam, Dynamic instabilities and turbulence of merged rotating Bose-Einstein condensates, *Phys. Fluids* **36**, 117121 (2024).
- [24] P. Mocz, M. Vogelsberger, V. H. Robles, J. Zavala, M. Boylan-Kolchin, A. Fialkov, and L. Hernquist, Galaxy formation with BECDM - I. Turbulence and relaxation of idealized haloes, *Mon. Not. R. Astron. Soc. RAS* **471**, 4559 (2017).
- [25] J. Lee, J. Kim, J. Jung, and Y. il Shin, Enhancement of damping in a turbulent atomic Bose-Einstein condensate (2025), arXiv:2502.07449 [cond-mat.quant-gas].
- [26] R. Ferrand, F. Sagraoui, D. Laveder, T. Passot, P. L. Sulem, and S. Galtier, Fluid Energy Cascade Rate and Kinetic Damping: New Insight from 3D Landau-fluid Simulations, *Astrophys. J.* **923**, 122 (2021).
- [27] I.-K. Liu, A. W. Baggaley, C. F. Barenghi, and T. S. Wood, Vortex avalanches and collective motion in neutron stars, *Astrophys. J.* **984**, 83 (2025).
- [28] V. Graber, N. Andersson, and M. Hogg, Neutron stars in the laboratory, *Int. J. Mod. Phys. D* **26**, 1730015 (2017).
- [29] S. Seveso, P. M. Pizzochero, F. Grill, and B. Haskell, Mesoscopic pinning forces in neutron star crusts, *Mon. Not. R. Astron. Soc.* **455**, 3952 (2016).
- [30] A. S. Bradley, R. K. Kumar, S. Pal, and X. Yu, Spectral analysis for compressible quantum fluids, *Phys. Rev. A* **106**, 043322 (2022).
- [31] P. Muruganandam and S. K. Adhikari, Fortran programs for the time-dependent Gross-Pitaevskii equation in a fully anisotropic trap, *Comput. Phys. Commun.* **180**, 1888 (2009).
- [32] R. K. Kumar, V. Lončar, P. Muruganandam, S. K. Adhikari, and A. Balaž, C and Fortran OpenMP programs for rotating Bose-Einstein condensates, *Comput. Phys. Commun.* **240**, 74 (2019).
- [33] V. Lončar, A. Balaž, A. Bogojević, S. Škrbić, P. Muruganandam, and S. K. Adhikari, CUDA programs for solving the time-dependent dipolar Gross-Pitaevskii equation in an anisotropic trap, *Comput. Phys. Commun.* **200**, 406 (2016).
- [34] M. Leadbeater, T. Winiecki, D. C. Samuels, C. F. Barenghi, and C. S. Adams, Sound emission due to superfluid vortex reconstructions, *Phys. Rev. Lett.* **86**, 1410 (2001).
- [35] M. Leadbeater, D. C. Samuels, C. F. Barenghi, and C. S. Adams, Decay of superfluid turbulence via Kelvin-wave radiation, *Phys. Rev. A* **67**, 015601 (2003).
- [36] A. Cidrim, A. C. White, A. J. Allen, V. S. Bagnato, and C. F. Barenghi, Vinen turbulence via the decay of multicharged vortices in trapped atomic Bose-Einstein condensates, *Phys. Rev. A* **96**, 023617 (2017).
- [37] P. W. Anderson and N. Itoh, Pulsar glitches and restlessness as a hard superfluidity phenomenon, *Nature* **256**, 25 (1975).
- [38] A. S. Bradley, C. W. Gardiner, and M. J. Davis, Bose-Einstein condensation from a rotating thermal cloud: Vortex nucleation and lattice formation, *Phys. Rev. A* **77**, 033616 (2008).
- [39] V. Khomenko and B. Haskell, Modelling pulsar glitches: The hydrodynamics of superfluid vortex avalanches in neutron stars, *Publ. Astron. Soc. Aust.* **35**, e020 (2018).
- [40] G. Howitt and A. Melatos, Antigligitches in accreting pulsars from superfluid vortex avalanches, *Mon. Not. R. Astron. Soc.* **514**, 863 (2022).
- [41] Y. O. Nikolaieva, A. O. Olashyn, Y. I. Kuriatnikov, S. I. Vilchynskii, and A. I. Yakimenko, Stable vortex in Bose-Einstein condensate dark matter, *Low Temp. Phys.* **47**, 684 (2021).